Biomaterials 2010
Doi:10.1016/j.biomaterials.2010.01.127

Crack arrest within teeth at the dentinoenamel junction caused by elastic modulus mismatch

Sabine Bechtle[1], Theo Fett[2], Gabriele Rizzi[3], Stefan Habelitz[4], Arndt Klocke[5], Gerold A. Schneider[1]*

[1]*Institute of Advanced Ceramics, Hamburg University of Technology, Denickestr. 15, D-21073 Hamburg, Germany*
[2]*Institute for Ceramics in Mechanical Engineering, Karlsruhe Institute of Technology (KIT), D-76021 Karlsruhe, Germany*
[3]*Institute for Materials Research II, Karlsruhe Institute of Technology (KIT), D-76021 Karlsruhe, Germany*
[4]*Department of Preventive and Restorative Dental Sciences, University of California, San Francisco, CA 94143, USA*
[5]*Department of Orofacial Sciences, University of California, San Francisco, CA 94143, USA*

*corresponding author: Gerold A. Schneider, g.schneider@tuhh.de

Abstract

Enamel and dentin compose the crowns of human teeth. They are joined at the dentinoenamel junction (DEJ) which is a very strong and well-bonded interface unlikely to fail within healthy teeth despite the formation of multiple cracks within enamel during a lifetime of exposure to masticatory forces. These cracks commonly are arrested when reaching the DEJ. The phenomenon of crack arrest at the DEJ is described in many publications but there is little consensus on the underlying cause and mechanism. Explanations range from the DEJ having a larger toughness than both enamel and dentin up to the assumption that not the DEJ itself causes crack arrest but the so-called mantle dentin, a thin material layer close to the DEJ that is somewhat softer than the bulk dentin. In this study we conducted 3-point bending experiments with bending bars consisting of the DEJ and surrounding enamel and dentin to investigate crack propagation and arrest within the DEJ region. Calculated stress intensities around crack tips were found to be highly influenced by the elastic modulus mismatch between enamel and dentin and hence, the phenomenon of crack arrest at the DEJ could be explained accordingly via this elastic modulus mismatch.

Key words: dentinoenamel junction, elastic modulus mismatch, stress intensity factor, enamel, dentin

1. Introduction

The dentinoenamel junction (DEJ) successfully interconnects two very dissimilar dental materials – the hard and wear-resistant cover-layer enamel and the softer and less mineralized dentin core. Dentin – the most abundant material within human teeth – is physically located between the exterior enamel layer and the interior pulp chamber. It is composed of ~ 47 vol% hydroxyapatite crystallites (HAP), ~ 20 vol% water and ~ 33 vol% proteins, mainly collagen-I fibrils [1]. The most prominent microstructural features in this material are the dentinal tubules - cylindrically shaped channels (1-2 μm in diameter) that span the entire dentin layer from the pulp chamber to the DEJ in a somehow S-curved manner [2]. The intertubular dentin is built by collagen fibrils that are reinforced with nanometre-scaled HAP crystallites [3]. Close to the DEJ these fibrils are oriented rather randomly, but orientation changes with increasing distance from the DEJ until fibrils form a network-like structure perpendicular to the dentinal tubules in the so-called bulk dentin [3]. Within bulk dentin, each dentinal tubule is surrounded by a highly mineralized cuff of peritubular dentin, ~ 1 μm in thickness [2]. Both, the thickness of this cuff and the tubule density itself decrease with decreasing distance to the DEJ and are almost absent within a 10-30 μm layer adjacent to the DEJ [4,5]. This layer is called ‘mantle dentin’.

Enamel is the hardest tissue in the human body and covers the dental crown. It is composed of ~ 85 vol% HAP crystals, ~ 12 vol% water and ~ 3 vol% organic matrix [1]. Bundles of nanometre-scaled HAP crystallites coated with proteins form the so-called enamel rods (about 5 μm in diameter) that run from the DEJ to approximately 6-12 μm below the tooth surface [6]. These rods are embedded within a continuous matrix - the interrod region - that is also formed by parallel aligned HAP crystallites and proteins [2]. However, the HAP crystallites within the interrod region are inclined at certain angles compared to adjacent enamel rods and thus, water and proteins are assumed to accumulate between rods and the interrod region due to the misalignment of enamel crystallites and increased porosity in this region [7]. Enamel can be divided into ‘outer enamel’ close to the tooth surface with the enamel rod long axes being straight and parallel and ‘inner enamel’ close to the DEJ where enamel rods are interwoven or decussated [2] with a smooth transition between both enamel types and an increasing amount of proteins towards the DEJ [8].

The optical DEJ visible in tooth cross sections appears as a scalloped line [9] with concavities on the enamel and convexities on the dentin side. The scallops are micrometer-scaled (25-100 μm within human teeth; [9]) and the amount and depth of the scallops was found to vary between species, type of teeth and between locations within single teeth [10]. Scalloping is assumed to improve the bonding strength between enamel and dentin by increasing the interfacial area [11]. DEJ bonding strength is also increased by type I collagen fibrils of dentin [12], 80-120 nm in diameter that appear to cross over the interface to be directly inserted into the highly mineralized structure of enamel.

During a tooth lifetime, cracks form within enamel due to singular overload events [9,13] typically without causing catastrophic tooth fracture. These cracks are found to start either at so-called ‘tufts’ (hypo-calcified fissures extending outward from the DEJ) growing towards the enamel surface or at flaws close to the tooth surface [14]. Latter cracks propagate towards the DEJ and are arrested there [13,15] or with limited penetration of [5,16] the underlying dentin core. This phenomenon has been known for years but there is little consensus within the literature regarding the cause of crack arrest at or close to the DEJ.
Older studies [17,18] focused on determining single fracture parameters for the DEJ region like the DEJ fracture toughness or work of fracture considering the DEJ being a unique

interface with corresponding unique fracture properties, e.g. a fracture toughness being higher than the one of enamel and dentin facilitating crack arrest [18].
However, the model concept of the DEJ being a sharp interface has been replaced during recent years by the conception of the DEJ as being a gradual interphase with smooth transitions of properties between enamel and dentin [4,5,9,16,19,20,21]. Most of these recent studies are focused on hardness and Young's modulus mappings across the DEJ from micro- or nanoindentation tests [9,16,20,21]. These maps show that e.g. the elastic modulus decreases from ~ 70 GPa within enamel to ~ 20 GPa within dentin over a transition zone (the so-called functional width of the DEJ) between 12-25 μm (determined by nanoindentation) and ~ 100 μm (determined by microindentation). Crack arrest consequently is no longer explained by single peak values (e.g. a peak toughness) of the DEJ but for example by the gradually increasing toughness from enamel to mantle dentin [16] with accompanying crack-tip shielding that originates from uncracked-ligament formation within the tough mantle dentin. Other researchers solely focus on the gradient dentin structure when trying to explain the crack arrest potential of the DEJ zone [4,5], e.g. by explaining crack arrest with the elastic modulus minimum of mantle dentin within which cracks might be trapped.

The focus of this study was on fracture mechanical testing of bulk samples containing the DEJ region with surrounding enamel and dentin and to investigate crack propagation and arrest in this area. For this purpose, bending experiments were conducted with bending bars including the DEJ and consisting of roughly equal amounts of enamel and dentin to analyse fracture behaviour within these samples. Comparable to the study of Lin and Douglas [18], samples were cracked perpendicular to the DEJ and stress intensities at the crack tip within the DEJ region were calculated. However, here, crack profiles were analysed in situ during mechanical loading and a new concept concerning the crack arrest phenomenon based on the mismatch of elastic moduli in enamel and dentin is proposed.

2. Materials and Methods

Materials

Bovine permanent mandibular incisors (n = 18) were used for the current study due to their larger size and flatness compared to human teeth facilitating the production of bending bars of ~ 1-2 x 1 x 10 mm^3 (width W x thickness B x length L) for mechanical testing techniques. It has been previously pointed out that bovine enamel exhibits a very similar microstructure to human enamel with same enamel rod size and shape, and similar amounts of constituents (HAP and organic components) [22,23]. Furthermore, it was observed by the authors in previous experiments that the enamel layer of bovine incisors can also be divided into inner and outer enamel with decussated and straight enamel rod arrangement, respectively, analogues to human enamel. Additionally, bovine and human dentin were found to exhibit very similar mechanical properties [24]. Rectangular shaped bending bars were prepared from entire tooth crowns by cutting with a slow speed saw and polishing. The teeth were cut to position the DEJ approximately in the middle of the samples running parallel to the bending bar long axis. Final polishing of all bending bar surfaces was done using a 600 grit SiC paper. The bending bar front side, on which crack propagation was visually monitored, was further polished using 1μm and 0,25 μm diamond suspension. A bovine incisor cross section with the sample site being indicated as well as a scheme of the extracted bending bars can be seen in Figure 1, dimensions of the prepared samples as indicated in Figure 1 are listed in Table 1; the different sample groups listed are defined in the next section ('Bending Tests'). The thickness d* of the inner enamel layer was estimated as the width over which Hunter-Schreger bands (light interference patterns that origin from decussated groups of enamel rods which are only

visible in the inner and not in the outer enamel layer [2]) are visible under the light microscope. As the inner enamel layer was approximated instead of measured precisely, one decimal point less is given compared to the other exactly measured dimensions.
Notched (n = 5) and un-nocthed (n = 13) specimens were tested. Two samples were notched beginning at the enamel surface, three at the dentin surface perpendicular to the DEJ up to about one half of the corresponding layer thickness (~ 400 μm) using a razor blade irrigated with 6 μm diamond suspension. Notches were then sharpened to a radius of ~ 20 μm using a razor blade irrigated with 1 μm diamond suspension.
Samples were stored in Hanks' Balanced Salt Solution (HBSS, Invitrogen, USA) at all times in order to minimize demineralization and, subsequently, changes in mechanical properties [25]. During preparation steps, samples were continuously irrigated with fluid. After preparation was completed, samples were stored in HBBS for at least 12 - 24h before mechanical testing. Samples were then removed from the solution and wiped. Mechanical testing in ambient air was completed within 30 minutes after removing the samples from HBSS.

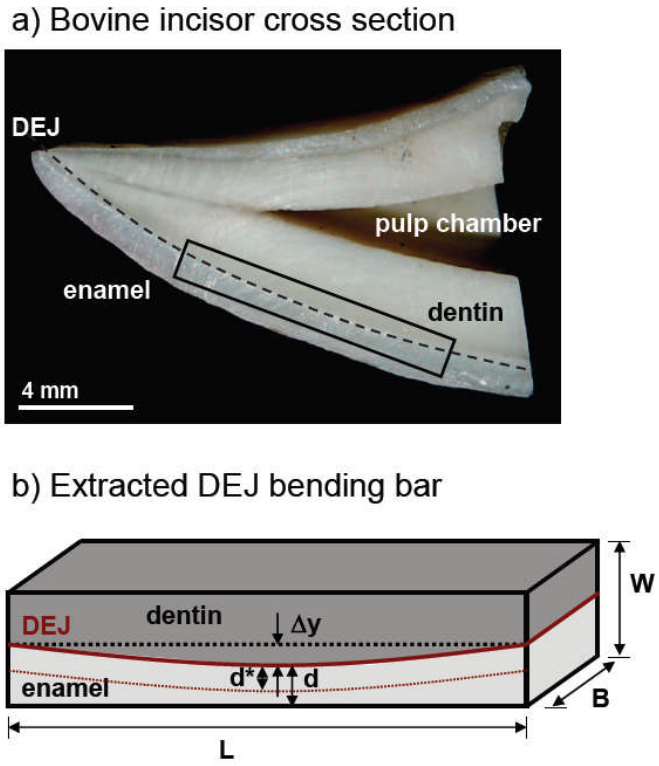

Figure 1: Cross section of a typical bovine incisor used can be seen in a) with the location of the extracted sample being indicated. A scheme of an extracted sample (not drawn to scale) is displayed in b). Due to the curved nature of the DEJ within bovine incisors, the DEJ deviates slightly from a straight line in some samples which is expressed via the parameter Δy which was determined for all samples, see Table 1. The smaller Δy, the flatter the DEJ contour. Enamel layer thickness d and inner enamel layer thickness d* which expands from the DEJ towards the sample surface over a region of about 400 μm were also determined. All sample dimensions indicated are listed in Table 1 except B and L which were 1 +/- 0,3 mm and 10 +/- 1 mm, respectively, in the samples prepared.

Table 1: Dimensions as indicated in Figure 1 for all samples which were prepared and tested. Sample width W, enamel layer width d, and deviation Δy of the DEJ from a straight line were determined on the sample front and sample back side to get an impression about the DEJ flatness throughout the sample thickness. The thickness of the inner enamel layer d* was estimated as the width over which Hunter-Schreger bands were visible under the light microscope. As the inner enamel layer was estimated instead of measured precisely, one decimal point less is given compared to the other dimensions. Samples were divided into four groups, for a detailed description see text; (1) enamel loaded in tension, un-notched; (2) enamel in tension, notched; (3) dentin in tension, un-notched; (4) dentin in tension, notched.

Sample group	sample	W front side [mm]	W back side [mm]	d front side [mm]	d back side [mm]	d* inner enamel [mm]	d/W front side	d/W back side	d/W average	Δy front side [mm]	Δy back side [mm]
1	1.1	1,01	1,04	0,65	0,54	0,4	0,64	0,51	0,58	0,08	0,10
	1.2	1,00	1,00	0,40	0,50	≥ 0,4	0,40	0,50	0,45	0,05	0,05
	1.3	1,40	1,43	1,10	0,75	0,6	0,78	0,52	0,65	0,01	0,06
	1.4	1,52	1,56	0,87	0,92	0,5	0,57	0,58	0,58	0,10	0,12
	1.5	1,43	1,51	0,97	0,80	0,5	0,67	0,52	0,60	0,06	0,03
	1.6	0,96	0,95	0,35	0,37	> 0,3	0,36	0,38	0,37	0,20	0,15
	1.7	1,86	1,9	1,10	1,05	0,8	0,59	0,55	0,57	~ 0	~ 0
	1.8	1,14	1,12	0,62	0,62	0,5	0,54	0,55	0,54	~ 0	0,01
	1.9	1,92	1,95	0,92	1,00	0,4	0,47	0,51	0,49	~ 0	0,01
2	2.1	1,71	1,69	0,97	0,83	0,3	0,56	0,49	0,52	0,04	0,06
	2.2	1,61	1,59	0,90	0,97	0,4	0,55	0,61	0,58	0,05	0,03
3	3.1	1,81	1,75	0,91	0,85	0,3	0,50	0,48	0,49	~ 0	0,10
	3.2	1,09	1,08	0,50	0,50	0,3	0,45	0,46	0,46	0,04	0,05
	3.3	1,01	1,00	0,46	0,48	0,4	0,45	0,48	0,46	0,15	0,20
	3.4	1,91	1,89	0,89	0,95	0,4	0,46	0,50	0,48	0,10	0,12
4	4.1	1,64	1,66	0,91	0,90	0,4	0,55	0,54	0,54	0,15	0,10
	4.2	1,73	1,73	1,00	0,95	0,4	0,57	0,54	0,56	0,03	0,03
	4.3	1,78	1,79	0,88	0,90	0,5	0,49	0,50	0,49	0,10	0,06
average		1,47 +/- 0,35	1,48 +/- 0,35	0,80 +/- 0,23	0,77 +/- 0,21	0,4 +/- 0,1	0,53 +/- 0,10	0,51 +/- 0,05	0,52 +/- 0,07	0,05 +/- 0,06	0,06 +/- 0,06

Bending Tests

Samples were mechanically tested using a custom-made three-point bending device equipped with a quartz load sensor (quartz dynamic load cell 9212, Kistler Instrumente GmbH) of high sensitivity (-11,3 pC/N) to measure the force acting on the sample, an inductive position encoder to measure the sample displacement and an optical microscope including a digital camera with 400x magnification for in situ visual crack length observations and documentation. The full loading range of the quartz load cell are 22 kN; the loads within the loading range applied within the experiments (0-50 N) were measured with 5% accuracy. A 3-point bending cell with a loading span S of 7 mm was used. The samples could be loaded manually by moving the upper support downwards. For a more detailed description of the bending device used see [26,27].

Samples were divided into four groups:

(1) un-notched bar, enamel side loaded in tension (9 samples)
(2) enamel side loaded in tension with the enamel side being notched perpendicular to the DEJ (2 samples)
(3) un-notched bar, dentin side loaded in tension (4 samples)
(4) dentin side loaded in tension with the dentin side being notched perpendicular to the DEJ (3 samples)

Within the notched sample groups, samples were loaded carefully and very slowly to achieve stable crack propagation away from the notch towards the DEJ. Crack profiles were documented. Un-notched samples were loaded until fracture occurred and force-displacement curves were monitored continuously as well as crack profiles were documented in situ (loading speed ~ $1{,}5*10^{-7}$ m/s; loading process was stopped at certain points for crack profile documentation).
After mechanical testing, a common light microscope was used for additional crack profile imaging.

Elastic Moduli Determination
Elastic moduli of enamel and dentin were necessary for stress intensity calculations (see next section) and were, therefore, determined by testing bending bars consisting entirely of enamel or dentin (6 samples each; loaded in orientations similar to the DEJ bending bars) in the previously described testing equipment and monitoring load-displacement curves that could be converted into stress-strain curves according to [28]:

$$\sigma = \frac{3PS}{2BW^2} \quad \text{and} \quad \varepsilon = \frac{4W(s - s^*)}{5S^2} \tag{1}$$

with P being the load acting on the sample, S the loading span, B the sample thickness, and W the sample width. s is the measured displacement and s* the displacement contribution of the bending device. Samples were loaded with a loading speed of approximately $1{,}5*10^{-7}$ m/s.
The displacement contribution of the bending device was determined by placing a very stiff, 10 mm thick alumina plate into the bending cell. A force-displacement curve was monitored and the bending device displacement was approximated by

$$s^* = 0{,}6 * P^{0,5} * \frac{\mu m}{N} \tag{2}$$

The elastic modulus E was determined within the linear-elastic deformation region of every sample due to

$$E = \frac{\Delta\sigma}{\Delta\varepsilon} \tag{3}$$

and the mean values of the two sample groups were determined.

Stress Intensity Calculations
Stress intensities around the crack tip during crack propagation within the bimaterial enamel-dentin bending bars were calculated according to the formula

$$K = \sigma_b F \sqrt{\pi a} \tag{4}$$

where σ_b is the formally computed bending stress

$$\sigma_b = \frac{3PS}{2BW^2} \tag{5}$$

with P being the applied load, S being the loading span, W being the sample width and B being the sample thickness as indicated in Figure 2a. F is a geometric function depending on sample and crack geometry. The stress intensity factor K is only defined for the case of the crack tip being located in one of the two materials and depends on the elastic modulus ratio E_1/E_2 of the two materials involved. The geometric function F of bimaterial bending bars with d/W = 0,5 was determined by the authors using Finite Element Analysis. Results for various E_1/E_2-ratios can be found in [29]. In Figure 2b & c, results for F are plotted for the elastic modulus ratios relevant for this study (for calculation of modulus ratios the elastic moduli determined in this study were used, see results) as well as the corresponding biaxiality ratios $\beta = T / (\sigma_b * F)$ according to Leevers and Radon [30] representing the first regular term of the stress field at a crack tip [F4], the T-stress T normalized by the geometric function F and the remote bending stress σ_b. Additionally, the values are listed in Table 2.

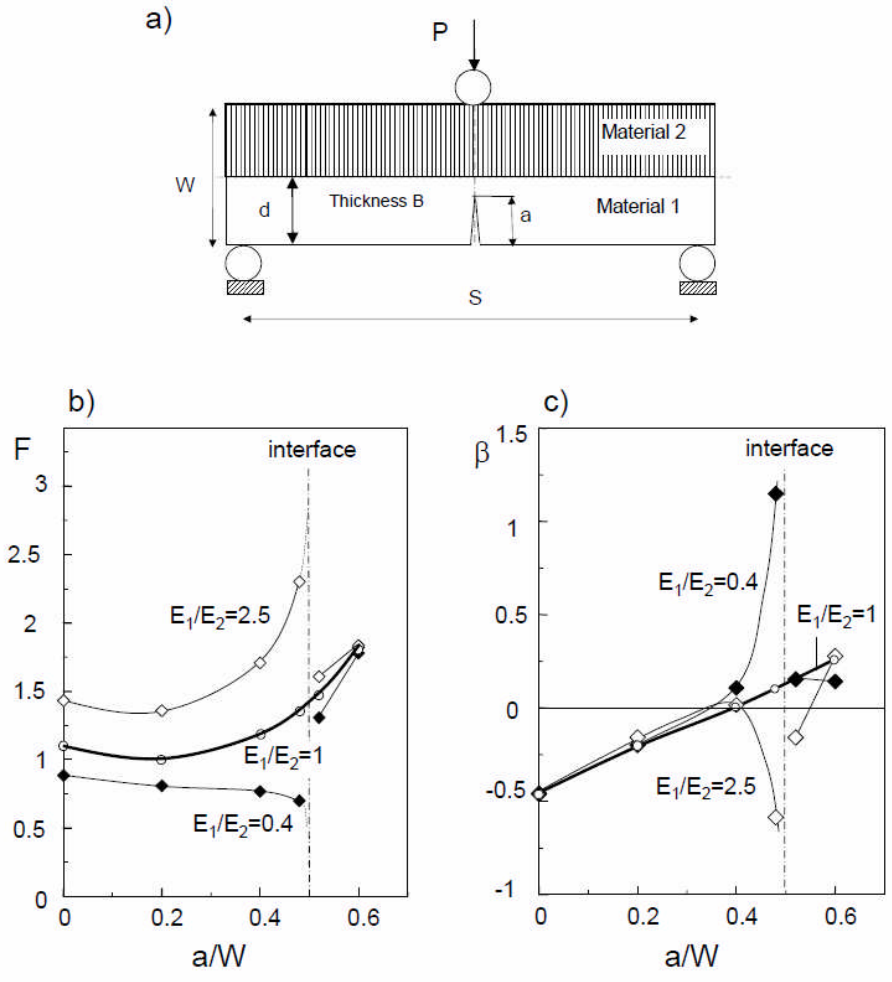

Figure 2: a) Schematic of notched specimen with dimensions b) Geometric function and c) Biaxiality ratio β representing the T-stress term ($\beta = T / (\sigma_b * F)$) for a bimaterial bar loaded in 3-point bending as shown in (a) with d/W = 0,5. Location of interface at a/W = 0,5. F and β in this case depend on the elastic modulus ratio E_1/E_2 of the two materials being involved and are listed in Table 2.

Table 2: Values for the geometric function F and the biaxiality ratio β representing the T-stress term for a bimaterial bar loaded in 3-point bending as shown in Figure 2a for d/W = 0,5 depending on elastic modulus ratio E_1/E_2 and normalized crack length a/W.

	F			β = T/(σ_b F)		
a/W	E_1/E_2 = 2.5	1	0,4	2,5	1	0,4
0	1,432	1,100	0,885	-0,469	-0,469	-0,469
0,2	1,358	1,001	0,809	-0,157	-0,206	-0,199
0,4	1,708	1,182	0,769	0,016	0,010	0,010
0,48	2,302	1,355	0,700	-0,585	0,098	1,149
0,52	1,607	1,472	1,307	-0,159	0,140	0,154
0,6	1,834	1,711	1,778	0,279	0,226	0,142

3. Results

The elastic moduli determined for enamel and dentin were 35,2 GPa +/- 5,6 GPa and 14,5 GPa +/- 2,9 GPa, respectively. Thus, the elastic modulus ratio for a DEJ bending bar with enamel in the tensile region was found to be 2,42, the one for a bar with dentin in the tensile region 0,41. For further calculations these ratios were approximated as 2,5 and 0,4.

Force-displacement curves and thus the fracture behaviour within un-notched samples with the enamel side loaded in tension can be divided into three groups, see Figure 3. Within sample group I (Figure 3a, 6 samples: 1.1, 1.4, 1.5, 1.7, 1.8, 1.9 as listed in Table 1) cracks formed at the enamel surface after the sample was loaded up to point 'A'. Cracks then propagated in an unstable manner but were arrested as the transition region between outer and inner enamel was reached ('A*'). The force acting on the samples sharply dropped during crack growth. Reloading the samples resulted in further unstable crack propagation (point 'B') and accompanying force reduction. Cracks were arrested at the DEJ ('B*'). Loading the samples again caused catastrophic fracture of the dentin layer (point 'C'). In sample group II (Figure 3b, 2 samples: 1.2 & 1.6 as listed in Table 1), cracks that formed at the enamel surface propagated directly up to the DEJ and were arrested there. In sample group III (Figure 3c, 1 sample: 1.3 as listed in Table 1) the initial unstable crack was arrested when entering the inner enamel layer. Further loading resulted in successive, stable crack propagation until catastrophic fracture occurred. The crack penetrated the dentin layer up to about 200 μm before unstable failure occurred.

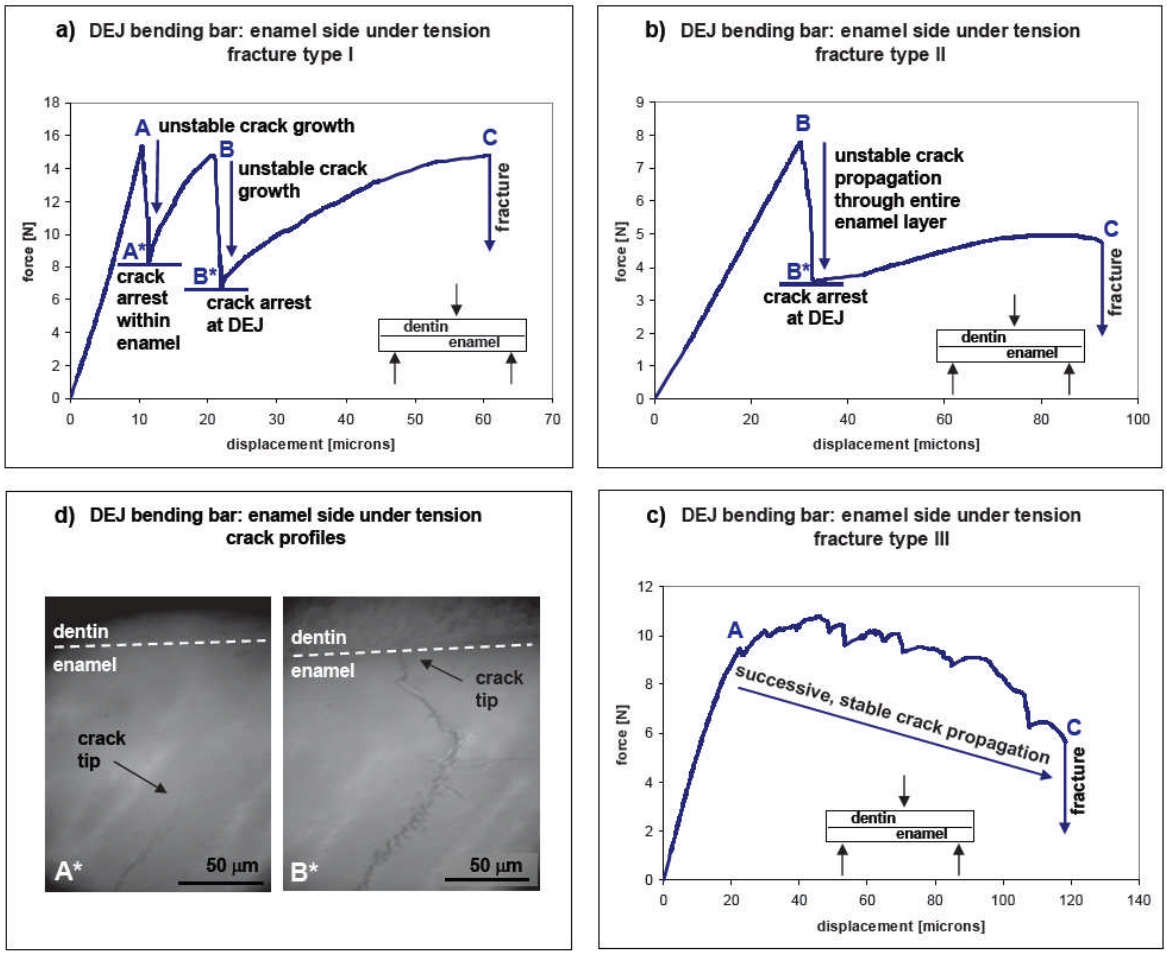

Figure 3: Typical force-displacement curves for un-notched DEJ bending bars with the enamel side loaded in tension (a) sample 1.4; b) sample 1.2; c) sample 1.3 as indicated in Table 1). Samples could be divided into three fracture types based on their force-displacement curves (a-c). At points 'A', unstable crack propagation occurred from the enamel surface up to the transition region between outer and inner enamel, where cracks were arrested ('A*'). At points 'B' unstable crack propagation could be observed with the cracks being arrested at the DEJ ('B*'). Catastrophic fracture occurred at points 'C'. Within sample groups I & II (a & b), crack propagation was always unstable and occurred in a stepwise manner. Within sample group III, crack propagation between points A and C occurred in a stable, successive manner. Within image d, in situ images illustrating crack profiles at points A* and B* of a sample out of group I are displayed.

Within notched DEJ bending bars with the enamel side loaded in tension, stable crack propagation could be realized within the enamel layer: cracks grew away from the notch towards the DEJ under almost constant loading - similar to fracture type III of the un-notched samples - and were arrested there. Comparable to the un-notched samples, further loading resulted in fracture of the dentin layer.

Crack arresting in notched and un-notched DEJ bending bars with the enamel side loaded in tension occurred within the "DEJ region". In some samples it seemed as if cracks were arrested directly at the optical DEJ (Figure 4a), in others cracks penetrated the underlying mantle dentin and were stopped after about 10-20 µm crack propagation within dentin independent of specific sample and loading type (Figure 4b). No specific conditions could be determined under which the cracks penetrate the dentin or not.

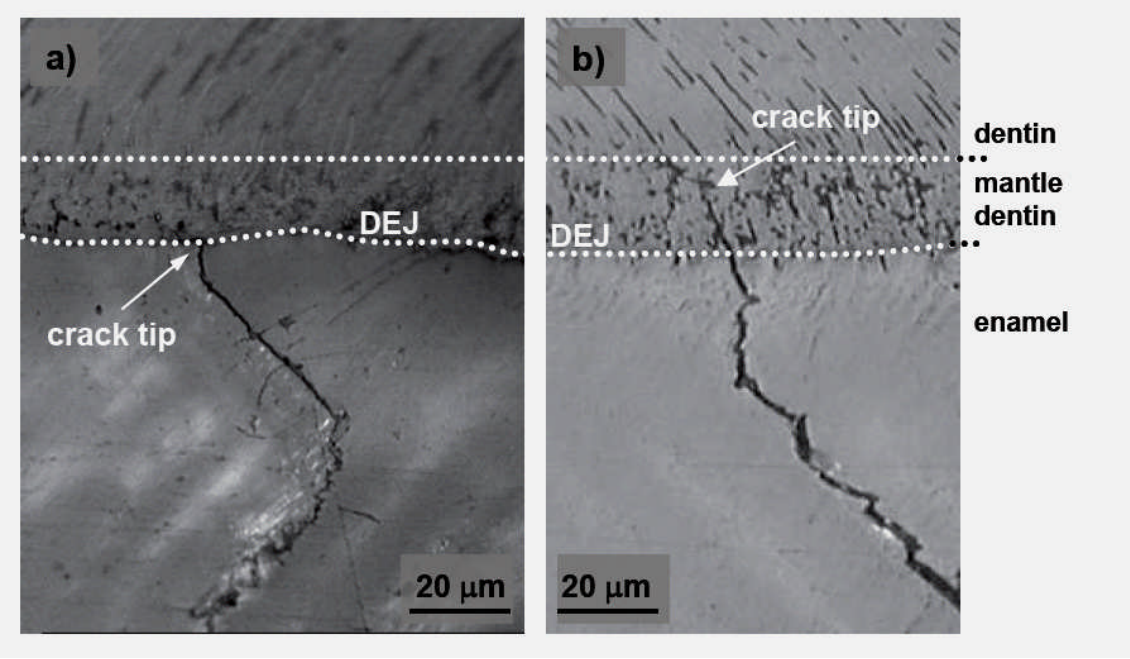

Figure 4: Crack arrest at the 'DEJ region' was observed in some samples to occur directly at the optical DEJ (a), in others cracks penetrated the mantle dentin and were arrested ~ 10-20 μm beyond the optical DEJ (b).

Figure 5 displays a typical force-displacement curve of an un-notched DEJ bending bar with the dentin side loaded in tension. Fracture occurred in a catastrophic manner after elastic and subsequent plastic deformation of the bending bar. No crack arrest within the DEJ region could be observed.

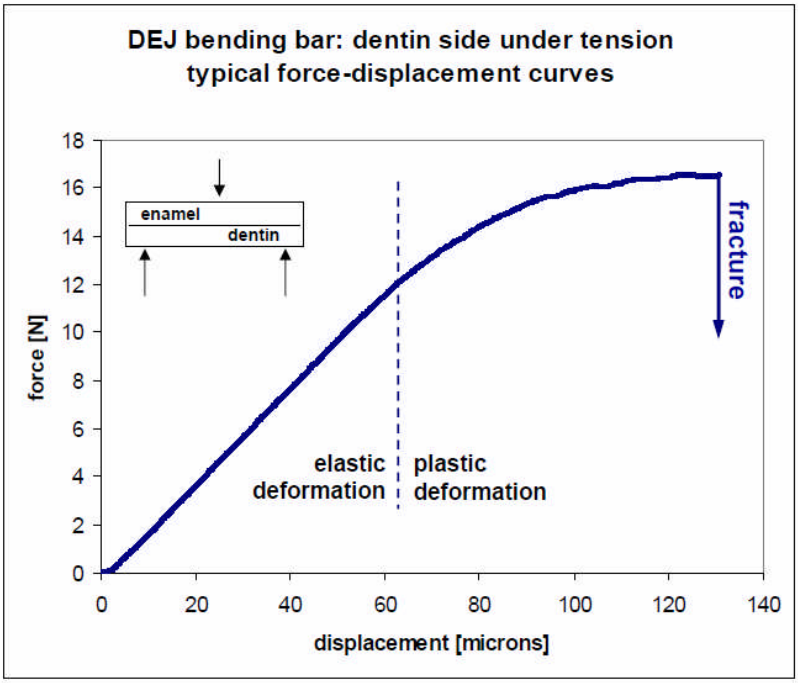

Figure 5: Representative force-displacement curve for an un-notched DEJ bending bar loaded with dentin under tension. Catastrophic fracture without crack arrest at the DEJ region occurred after pronounced elastic and plastic deformation.

Among notched DEJ bending bars with the dentin side loaded in tension, cracks propagated simultaneously in a stable manner within dentin and enamel: Crack propagation started away from the notch towards the DEJ and at the same time, a crack was formed at the DEJ growing away from the interface within the enamel layer (see Figure 6a). In two samples, those two cracks coalesced (Figure 6b) whereas in one sample, a 'DEJ uncracked ligament' formed, bridging the two cracks and keeping the two fractured sample parts together (Figure 6c).

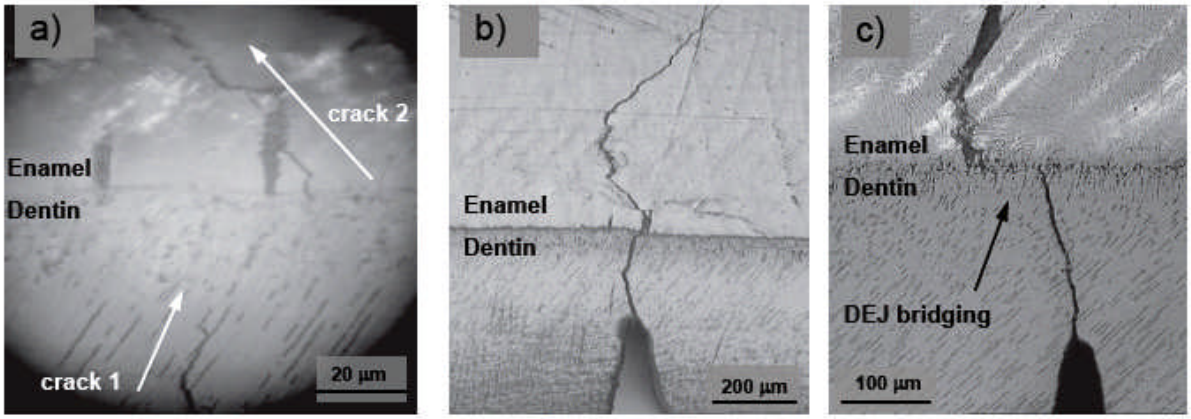

Figure 6: Within notched DEJ bending bars with dentin side under tension, crack propagation occurred simultaneously within dentin and enamel as can be seen within the in situ image (a). The same sample after testing was completed is shown in (b): The two cracks coalesced, building one continuous crack profile. Within another sample, the two cracks did not meet at the DEJ and thus, the DEJ formed an unbroken ligament between cracks, keeping the two fractured sample parts together (c).

Summarizing the results of all tested sample groups it can be noted that in almost all samples cracks crossed the DEJ at angles between 45 and 90° independent of the material layer the crack started in or of the kind of crack propagation (unstable or stable). Separation of the DEJ was only observed in two samples: in one sample, the DEJ was sheared as a consequence of crack opening. In the other sample, the DEJ cracked while the main crack was crossing the interface at 45° (see Figure 7). In all other samples cracks crossed the interface without affecting the DEJ.

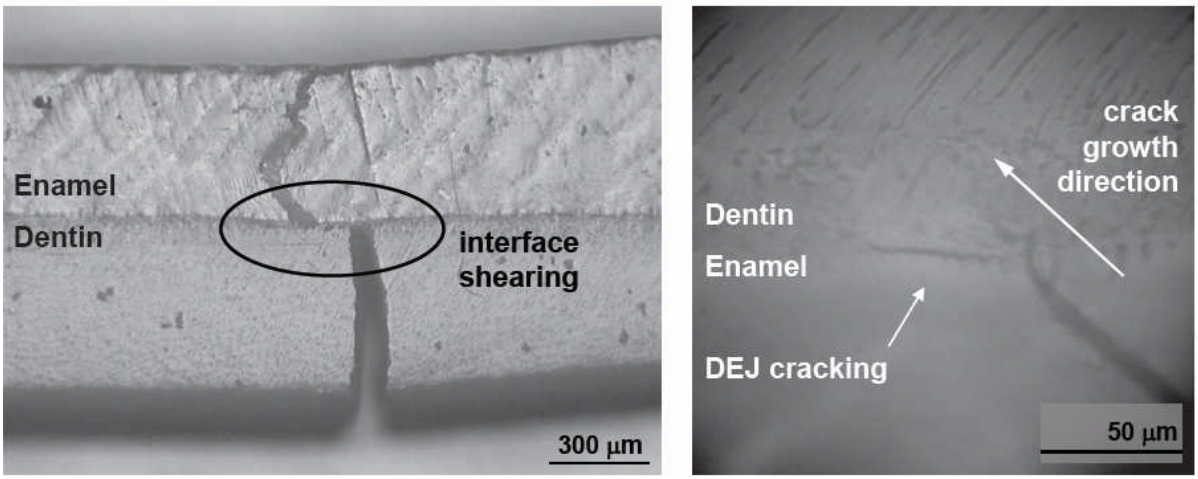

Figure 7: Here, the two samples are shown where the DEJ was affected during crack propagation: in a) the interface sheared as a consequence of crack opening; in b) the DEJ cracked while the main crack was crossing the interface at ~ 45°. In all other samples tested, the DEJ stayed intact during mechanical testing.

In Figure 8, typical profiles of fractured un-notched samples are shown which were loaded with enamel (a) and dentin (b) in tension, respectively. Within dentin, cracks propagated in a straight line in some samples (a), in others the crack profile was arched or curved (b). Within the enamel layer, cracks propagated at 45° to the sample surface and were deflected by 90° in the transition region between inner and outer enamel (a, b). Cracks propagating within enamel towards the DEJ (b) were deflected a second time close to the DEJ in most samples so that cracks penetrated into dentin under angles between 45 and 90°. Notched samples exhibited similar crack profiles with the notch being the only distinguishable element (see for comparison Figure 6b and Figure 7).

For stress intensity calculations for samples with the enamel side loaded in tension some corrections were necessary since the true crack profile displayed in Figure 8b differed largely from the idealized straight crack in Figure 2a that was used for geometric function F determination.
Similar to the suggestions of Noda and Oda [31] the deflected and kinked crack within the enamel layer was approximated by a slant crack exhibiting the same inclination angle as the true crack close to its tip. Hence, the double kinked crack within the enamel layer was approximated by a slant crack with the same slope as the kink close to the DEJ, see Figure 8. Furthermore (as this could not be verified during experiments due to restrictions of the experimental setup), it was assumed that crack formation was initiated at the sample surface loaded in tension exactly between the loading points of the bending cell where the tensile bending stress has its maximum. Thus, the tip of the approximated slant crack close to the DEJ shows a certain misalignment x from the location of maximum bending stress σ_b (see Figure 8c) as samples were tested in 3-point bending where the bending moment (thus, the bending stress) varies linearly over the loading span S. The equations available for calculations, however, require a constant bending moment (as commonly realized in 4-point bending). Misalignments x of the crack tip close to the DEJ from maximum stress would be around 200 μm if cracks were initiated at the centre between loading points. This would result in true stresses at the crack tip of around $0{,}94\sigma_{max}$. However, as we could not be absolutely sure concerning the crack initiation point and the real misalignment x we did not account for this in our calculations, what slightly reduces the accuracy of the calculated stress intensity values.

The geometric functions $F_{I,II}$ for the approximated slant crack could then be express by [36]

$$F_{I,slant} = F\,[\cos^3(\tfrac{1}{2}\varphi) + 0.17845\beta\sin^2\varphi/\sqrt{\cos\varphi}] \quad (6)$$

$$F_{II,slant} = F[\cos^2(\tfrac{1}{2}\varphi)\sin(\tfrac{1}{2}\varphi) - 0.2182\,\beta\sin\varphi\sqrt{\cos\varphi}] \quad (7)$$

The mode-II stress intensity component (in-plane shear) in this case is induced due to oblique crack propagation. F is the geometric function of a sample with straight crack loaded in 3-point bending (see Figure 2) and β is the biaxiality ratio. Values for β and F were selected from Table 2 for the determined elastic modulus ratio of 2,5 for DEJ bending bars with enamel in the tensile region.

For stress intensity calculations, un-notched bending bar samples were chosen with enamel loaded in tension, which had a d/W ratio closest to 0,5 (0,45-0,60) and exhibited the most uniform DEJ profiles through sample thickness and length ($\Delta y \leq 0{,}1$ mm, difference between Δy of sample front and back side $\leq 0{,}03$ mm). Additionally, the angle of the last kink close to the DEJ had to be very well visible for crack profile approximation. Samples 1.1, 1.2, 1.5, 1.7, and 1.8 fulfilled all criteria. Stress intensities were calculated at 3 points: At points 'B*' in the force-displacement curves (see Figure 3a & b), cracks stopped at the DEJ at a certain load, which was used to calculate stress intensities close to the DEJ while cracks were approaching the interface (a/W = 0,48). The same force values were used to calculate stress intensities acting around the crack tips when cracks were arrested at or slightly beyond the DEJ (a/W = 0,52). At points C (see Figure 3a & b), catastrophic fracture of samples occurred. Stress intensities causing these fractures were calculated for the corresponding fracture forces. Results are displayed in Table 3.

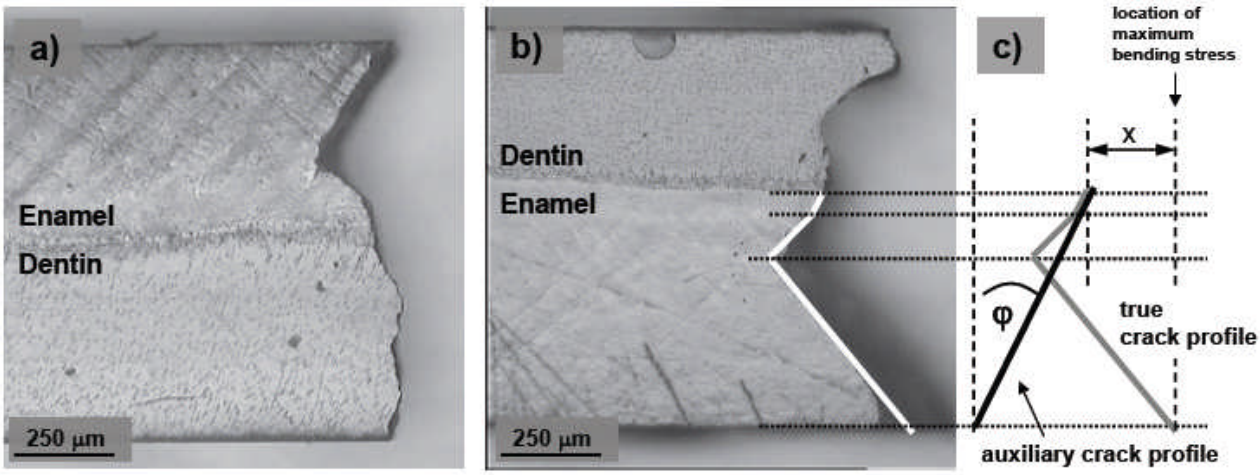

Figure 8: Typical profiles of fractured un-notched samples where a) the dentin side was loaded in tension and b) the enamel side was loaded in tension. Note that 90° crack deflection occurred in both sample types at the transition from outer to inner enamel and that crack propagation within enamel occurred at an inclination of 45° within large parts of the samples. Cracks approaching the DEJ from the enamel side were again deflected close to the DEJ so that crack penetration into dentin occurred under angles between 45 and 90° (b). In c), the auxiliary crack profile is shown that was used as an approximation for the deflected and kinked enamel crack for stress intensity calculations. Similar to the suggestions of Noda and Oda [31], such a crack can be approximated by a simple straight crack exhibiting the same slope as the true crack in the near-tip region.

Table 3: Stress intensities around the crack tip during crack propagation and arrest within un-notched bending bars with enamel side loaded in tension. Values are given for the crack tip approaching the DEJ, being arrested at or closely behind the interface and for final fracture. For stress intensity calculations, the corresponding force values were chosen from the load-displacement curves (see Figure 3), values for the geometric function were taken from Table 2 for appropriate a/W ratios. True crack profiles were approximated by a slant crack with angle φ (see Figure 8).

	Inclination angle of approximated slant crack	**Crack approaches the DEJ:** a/W = 0,48 Force: B*		**Crack stops at the interface:** a/W = 0,52 Force: B*		**Fracture of dentin layer:** a/W = 0,52 Force: C	
sample	**φ**	**K_I**	**K_{II}**	**K_I**	**K_{II}**	**K_I**	**K_{II}**
1.1	2	3,87	0,08	2,63	0,05	3,43	0,07
1.2	20	3,52	0,76	2,42	0,47	2,90	0,56
1.5	5	3,12	0,17	2,11	0,10	3,25	0,16
1.7	45	3,30	1,82	2,42	1,09	4,15	1,88
1.8	45	3,56	1,96	2,60	1,18	3,12	1,42
mean value	23	3,47	0,97	2,44	0,58	3,37	0,81
std. dev.	18	0,16	0,94	0,01	0,57	0,15	0,68

4. Discussion

In agreement with other researchers [16,17] we observed that cracking directly along the DEJ occurs very rarely. The DEJ seems to be a very well and strongly bonded interface and is not the weakest link like in many artificial bimaterial systems.

The uncommon crack profiles of the cracks within enamel propagating at 45° angles were most likely caused by oblique enamel rod orientation within the bending bars prepared. In a previous study [27] we found that in longitudinal oriented enamel with very straight and parallel rods (this orientation corresponds to the orientation of the outer enamel layer in the DEJ bending bars tested in this study), cracks are forced on oblique paths due to oblique rod alignment with the cracks favourably propagating within the protein-rich interrod region. In the inner enamel layer, where rods are no longer determining crack paths so strictly as they are decussated and provide several possible crack paths, the macroscopic 45° shear fracture might potentially be enhanced via a protein shearing mechanism as was already proposed by us in [27]. It is interesting that in all samples cracks were deflected by 90° at the transition between outer enamel and inner enamel. Beside crack deflection, microcracking, enamel rod bridging and protein bridging could be observed to impede crack propagation within inner enamel [27,32]. The microstructural change from outer to inner enamel has two effects: a rising toughness [32] and a change in crack propagation direction as observed. Therefore the crack loading in terms of K_I and K_{II} changes as well as the crack resistance. Both effects resulted in a first initial crack arrest before the DEJ in samples of fracture type I (Figure 3a). Thus, in a lifetime of a tooth, cracks in the enamel are not only shielded from the dentin core by crack arrest at the DEJ but also by cracks arresting due to introduction of rod decussation starting at the outer-inner enamel transition. However, within samples of fracture type II

(Figure 3b), this initial crack arrest was absent. Looking at the sample dimensions of the samples out of this group (1.2 & 1.6, Table 1) the reason for this is obvious: The inner enamel layer d* expands over the entire enamel layer d in these two samples. The entire outer enamel layer and hence, the outer-inner enamel transition was removed during sample preparation. In all other samples, the enamel layer consists of both enamel types. Sample 1.3 is the only one that fractured in a successive, stable manner (Figure 3c). Unfortunately, this special type of failure cannot be linked directly to unique sample dimensions or an anomalous crack profile. We at this point can only speculate: maybe, this sample contained (as a result of loading during lifetime) an extraordinary number of microcracks which coalesced successively during testing.

At this point it should also be noted, that the force-displacement curves shown (Figures 3 & 5) are not normalized according to sample dimensions. Thus, no direct information concerning stiffness or consumed fracture energy can be extracted out of these diagrams. However, we decided to show the measured force-displacement curves directly without calculating stresses and strains incorporating sample dimensions as it is quite complicated to calculate physically meaningful bending stresses for bimaterial bending bars.

The kink-formation in enamel close to the DEJ within samples loaded with enamel in the tensile region (see Figure 8) is possibly caused by the acting T-stress field: within inner enamel, crack direction is no longer that strongly determined by enamel rod orientation as domains of enamel rods are interwoven in this region providing several possible crack propagation directions. As can be seen in Figure 2c**,** the biaxiality ratio β (and thus, the T-stress term) in this region for $E_1/E_2 = 2{,}5$ (enamel in the tensile region) becomes negative. According to [33] negative T-stresses enhance crack path stability, i.e. straight crack propagation – resulting in kinks at the crack tip reducing the crack path inclination angle. Another important point to mention concerning the T-stresses is that interface cracking is suppressed for $T < 0$ because the interface ahead of a crack tip is then under compression. In contrast, interface cracking is enhanced for $T > 0$. However, bonding strength of the DEJ seems to be as high that even under enhanced possibility of interface cracking ($\beta > 0 \rightarrow T > 0$, dentin side under tension, see Figure 2c) hardly any cracking occurred along the DEJ.

The most interesting finding of this study was that cracks are only arrested at the DEJ if cracks approach the DEJ from the enamel side. It has been assumed that cracks arrest at the interfacial zone due to the larger toughness of dentin if compared to enamel. Recent results, however, showed that the toughness of enamel exceeds that of dentin [27,32,36]. Thus, toughness differences may not be the appropriate parameter to explain the crack arrest phenomenon. Other researchers like Tesch et al [5] speculated that cracks might be trapped within the elastic modulus minimum of the mantle dentin layer. The indentation elastic modulus of human mantle and bulk dentin were determined by them to be 19,5 GPa and 26,5 GPa, respectively. This modulus increase from mantle to bulk dentin is approximately 35% whereas the drop in elastic modulus from human enamel to dentin is as large as 70-80% and occurs over a width of only several micrometers [19] (elastic modulus of human enamel close to the DEJ is around 80 GPa if determined via indentation methods [8]). Thus, we suggest that the elastic modulus mismatch between enamel and dentin has the larger influence on crack propagation. However, the elastic moduli that were determined in our study for bovine enamel and dentin were much smaller than the values derived from indentation methods on human teeth (Enamel: 35,2 GPa, Dentin: 14,5 GPa) with the difference between indentation and bending modulus being around 50%. This can be ascribed to a size effect that was already observed by He et al [34] and Ang et al [35] with the elastic moduli in enamel decreasing with larger sample volumes being tested: in larger testing volumes, larger amounts of microcracks and flaws are comprised, decreasing the stiffness and hence, the elastic modulus of a material. Variations between species (human verse bovine) leading to a difference as large as 50% in

elastic moduli are rather unlikely: indentation moduli for bovine enamel for example are also around 80 GPa [35] and hence, are in good agreement with data for human teeth [8].
For stress intensity calculations the elastic moduli determined in this study were used for geometric function determination with the simplification of enamel and dentin having isotropic and gradient-free elastic moduli. Again, we think this simplification is appropriate as the difference between enamel and dentin (70-80%) is much larger than the internal elastic moduli variations within those two materials (~ 22% within enamel [8] and ~ 35% within dentin [5]).
Mode I stress intensities around cracks within enamel approaching the DEJ were around 3,47 $MPa*m^{1/2}$ close to the interface which is in very good agreement with values determined for pure enamel bending bars after ~ 400 μm crack extension within the inner enamel region [36] where toughening takes place [32]. Due to the elastic modulus mismatch of enamel and dentin, the geometric function (Figure 2b) drops sharply at the interface – consequently, mode I stress intensities dropped to ~ 2,44 $MPa*m^{1/2}$ when cracks crossed the DEJ. Cracks were arrested as the driving force for crack propagation, the stress intensity, was no longer high enough to fulfil the crack propagation criterion $K \geq K_C$ (where K is the stress intensity acting around the crack tip and K_C is the fracture toughness of the material). If samples were further loaded, catastrophic fracture finally occurred (Figure 3a & b, point 'C') – stress intensities around 3,37 $MPa*m^{1/2}$ were necessary to cause this catastrophic fracture. These stress intensities at final fracture were markedly larger than stress intensities necessary to cause initial crack propagation within dentin which were determined to be around 1 $MPa*m^{1/2}$ for pure dentin bending bars [36]. However, due to protein and enamel rod bridges that likely span the cracks within enamel [27,32], additional stresses will be required to break these bridges and to continue to drive the crack through dentin. Furthermore, true stress intensities at the crack tip in dentin might be lower than the calculated 3,37 $MPa*m^{1/2}$ due to dissipation processes correlated with the occurring plastic deformation (see force-displacement curves in Figure 3a & b) that were neglected in our calculations.
In addition to the neglected plastic deformation some more approximations have been made which might limit the accuracy of the presented stress intensities: Firstly, the slightly curved shape of the DEJ was approximated by a straight line (see Figure 1). To minimize errors that could arise from this approximation, only samples with small Δy were chosen for stress intensity calculations. Secondly, the ratio of the enamel layer d to entire sample width W was not exactly 0,5 but ranged from 0,45 to 0,6. As already mentioned in the results section, the maximum bending stress was used for calculations although the crack tip at the DEJ might be misaligned a bit resulting in a reduced true stress of around 0,94 times the maximum bending stress. However, if errors are induced due to this approximation they are of same amount for the stress intensity values for cracks approaching the DEJ and for values for crack arrest within each sample (for both values, same forces are used for calculation): so that the relative changes in stress intensity at the DEJ for each sample should be correct. The double kinked cracks were approximated by slant cracks according to a method proposed by Noda and Oda [31] – this should not result in a lack of accuracy.
However – though a bunch of approximations and estimations had to be used for stress intensity calculations – the calculated values seem to be quite reasonable. As mentioned previously, the values for cracks approaching the DEJ from the enamel side are in very good agreement with values measured in entire enamel bending bars for comparable crack extension in the inner enamel layer [see 36]. This is quite a good proof for us that our calculations should be correct and approximations that had to be used were acceptable.
Mode II values were induced due to oblique crack propagation (not due to external loading conditions) and show a larger scatter than the mode I values. The mode II values increase with larger inclination angle φ. This angle was found to range from 2 to 45°, and so the mode II values also cover a wide range. Since the mode I values for the different angles are more

uniform and far higher than the mode II values, they most likely are the main driving forces for crack propagation in the bimaterial DEJ bending bars.
In the case of dentin exposed to tensile stresses, the geometric function sharply increases at the DEJ (see Figure 2b). A crack approaching the DEJ from the dentin side will see an increased stress intensity after crossing the DEJ – and thus, will be enhanced to propagate through the sample. The crack in this case would only stop if the increase in the material's fracture toughness across the interface would be larger than the increase in stress intensity due to the elastic modulus mismatch. Obviously, the latter is not the case in dentin-enamel bimaterial bending bars and hence, samples fractured without crack arrest.
In notched samples with dentin loaded in tension, a crack within enamel was already formed before the crack approaching the DEJ from the dentin side actually reached the DEJ (see Figure 6). This might have the following reason: within an un-cracked bending bar of a homogeneous material, the bending stress along the sample cross section has its maximum at the surface loaded in tension and decreases continuously along the sample width. Within the middle of the sample, the bending stress is zero and on the opposite sample side the bending stress is a compressive stress of the same absolute value as the maximum tensile stress. Due to the higher elastic modulus of enamel, the location of the so-called neutral axis (where the bending stress is zero) within a DEJ bending bar with dentin loaded in tension is shifted from the middle of the sample – the DEJ – inside the enamel layer so that the DEJ and the enamel layer adjacent to the DEJ are loaded in tension. Furthermore, the tensile stress has a local maximum within enamel close to the DEJ as a consequence of the discontinuous elastic modulus [37]. Cracks in enamel might have been initiated at flaws (like microcracks or tufts) close to the DEJ that were exposed to these tensile stresses (assuming that the stress field of the crack approaching the DEJ from the dentin side can be neglected due to sufficient distance from the DEJ) – resulting in the observed simultaneous crack propagation in dentin and enamel.
Considering the unique crack profiles of the tested DEJ samples in context of the shifted neutral axes it might also be possible that these crack profiles are not only influenced by internal enamel rod structure as explained previously but also by tensile and compressive stress distribution. In Figure 8 it can be seen that cracks are deflected within enamel in both sample types tested (enamel in compression (a) and tension (b)). If enamel is tested in compression, the neutral axis is shifted away from the sample centre (ideally the DEJ) into the enamel layer. Crack deflection occurs roughly where the compression part of the sample begins. If enamel is tested in tension, the neutral axis is also shifted into the enamel layer and crack deflection again occurs where the neutral axis might be located. Comparable to ceramic materials, the crack deflection within enamel could arise from compression curl formation. However, as oblique crack propagation in enamel and crack deflection at the outer-inner enamel transition region could be observed by the authors in various experiments [27,36 & unpublished work done by the authors] as well as such deflection can also be seen in [32] within a compact tension specimen the explanation related to enamel rod structure stated above seems to be more likely.

5. Conclusion

By investigating crack propagation and arrest within DEJ bending bars and correlated crack profile analysis it was observed that crack arrest only occurs if cracks approach the DEJ from the enamel side. If cracks are induced from the dentin side, samples fractured after elastic and some amount of plastic deformation. The phenomenon of crack arrest was explained via the elastic modulus mismatch between enamel and dentin that was found to highly influence stress intensities around crack tips in the DEJ bimaterial bending bars. This study suggests that the DEJ itself is a very well-bonded and strong interface since cracking along the DEJ occurred rather seldom.

Acknowledgement

This paper is published in **Biomaterials 2010; doi:10.1016/j.biomaterials.2010.01.127**

Literature

1. Lussi, A. Dental Erosion – from Diagnosis to Therapy. 1st ed. Basel: Karger; 2006.
2. Ten Cate, AR. Oral Histology: Development, Structure and Function. 7th ed. St. Louis: Mosby; 2003.
3. Kinney JH, Pople JA, Marshall GW, Marshall SJ. Collagen orientation and crystallite size in human dentin: a small angle x-ray scattering study. Calcif Tissue Int 2001; 69: 31-7.
4. Zaslansky P, Friesem AA, Weiner S. Structure and mechanical properties of the soft zone separating bulk dentin and enamel in crowns of human teeth: insight into tooth function. J Struct Biol 2006; 153: 188-99.
5. Tesch W, Eidelmann N, Roschger P, Goldenberg F, Klaushofer K, Fratzl P. Graded microstructure and mechanical properties of human crown dentin. Calcif Tissue Int 2001; 69: 147-57.
6. Gray H, Bannister LH, Berry MM, Williams PL. Gray's Anatomy: The Anatomical Basis of Medicine & Surgery. 38th ed. Churchill Livingstone; 1995.
7. Maas MC, Dumont ER. Built to last: the structure, function and evolution of primate dental enamel. Evol Anthrop 1999; 8: 133-52.
8. Cuy JL, Mann AB, Livi KJ, Teaford MF, Weihs TP. Nanoindentation mapping of the mechanical properties of human molar tooth enamel. Arch Oral Biol 2002; 47(4): 281-91.
9. Marshall SJ, Balooch M, Habelitz S, Balooch G, Gallagher R, Marshall GW. The dentin-enamel junction – a natural, multilevel interface. J Eur Ceram Soc 2003; 23: 2897-904.
10. Whittaker DK. The enamel-dentin junction of human and macaca irus teeth: a light and microscopic study. J Anat 1978; 125: 323-35.
11. Douglas WH. Clinical status of dentine bonding agents. J Dent 1989; 17: 209-15.
12 Lin CP, Douglas WH, Erlandsen SL. Scanning electron microscopy of type I collagen at the dentin-enamel junction of human teeth. J Histochem Cytochem 1993; 41: 381-8.
13. Chai H, Lee JJW, Constantino P, Lucas PW, Lawn B. Remarkable resilience of teeth. Proc Natl Acad Sci 2009; 106: 7289-93.
14. Lee JJW, Kwon JY, Chai H, Lucas PW, Thompson VP, Lawn BR. Fracture modes in human teeth. J Dent Res 2009; 88: 224-8.
15. Xu HHK, Smith DT, Jahanmir S, Romberg E, Kelly JR, Thompson VP, Rekow ED. Indentation damage and mechanical properties of human enamel and dentin. J Dent Res 1998; 77: 472-80.
16. Imbeni V, Kruzic JJ, Marshall GW, Marshall SJ, Ritchie RO. The dentin-enamel junction and the fracture of human teeth. Nat Mater 2005; 4: 229-32.
17. Rasmussen ST. Fracture Properties of human teeth in proximity to the dentinoenamel junction. J Dent Res 1984; 63: 1279-83.
18. Lin CP, Douglas WH. Structure-property relations and crack resistance at the bovine dentin-enamel junction. J Dent Res 1994; 73: 1072-8.
19. Habelitz S, Marshall SJ, Marshall GW, Balooch M. The functional width of the dentino-enamel junction determined by AFM-based nanoscratching. J Struct Biol 2001; 135:294-301.
20. Urabe I, Nakajima M, Sano H, Tagami J. Physical properties at the dentino-enamel junction region. Am J Dent 2000; 13: 129-35.
21. Balooch G, Marshall GW, Marshall SJ, Warren OL, Asif SAS, Balooch M. Evaluation of a new modulus mapping technique to investigate microstructural features of human teeth. J Biomech 2004; 37: 1223-32.
22. Oesterle LJ, Shellhart WC, Belanger GK. The use of bovine enamel in bonding studies. Am J Ortho 1998; 114: 514-20.
23. Sanches RP, Otani C, Damiao AJ, Miyakawa W. AFM characterization of bovine enamel and dentine after acid etching. Micron 2009; 40: 502-6.

24. Sano H, Ciucchi B, Matthews WG, Pashley DH. Tensile properties of mineralized and demineralized human and bovine dentin. J Dent Res 1994; 73:1205-11.
25. Habelitz S, Marshall GW, Balooch M, Marshall SJ. Nanoindentation and storage of teeth. J Biomech 2002; 35: 995-8.
26. Jelitto H, Felten F, Swain MV, Balke H, Schneider GA. Measurement of the total energy release rate for cracks in PZT under combined mechanical and electrical load. J Appl Mech 2007; 74: 1197-211.
27. Bechtle S, Habelitz S, Fett T, Klocke A, Schneider GA. The fracture behaviour of dental enamel. Biomaterials 2010; 30: 375-84.
28. DIN EN 843-1: Advanced technical ceramics – Mechanical properties of monolithic ceramics at room temperature – Part 1: Determination of flexural strength. Deutsches Institut für Normen eV, Berlin: Beuth Verlag; 2006.
29. Fett T. Stress intensity factors, T-stresses, Weight function (Supplement Volume). Universitätsverlag Karlsruhe; 2009.
30. Leevers PS, Radon JC. Inherent stress biaxiality in various fracture specimen geometries. Int J Fract 1982; 19; 311-25.
31. Noda NA, Oda K. Effect of curvature at the crack tip on the stress intensity factor for curved cracks. Int J Fract 1993: 64; 239-49.
32. Bajaj D, Arola DD. Role of prism decussation on fatigue crack growth and fracture of human enamel. Acta Biomater 2009; 5: 3045-56.
33. Cotterell B, Rice JR. Slightly curved or kinked cracks. Int J Fract 1980; 16: 155-69.
34. He LH, Swain MV. Understanding the mechanical behaviour of human enamel from its structural and compositional characteristics. J Mech Behav Biomed Mater 2008; 1: 18-29.
35. Ang SF, Bortel EL, Swain MV, Klocke A, Schneider GS. Size dependant elastic/inelastic behaviour of enamel: from millimetre to nanometre length scales. Biomaterials, *in press.*
36. Bechtle S, Fett T, Rizzi G, Habelitz S, Schneider GA. Mixed-mode stress intensity factors for kink cracks with finite kink length loaded in tension and bending – application to dentin and enamel. J Mech Behav Biomed Mater; *in press.*
37. Noda NA, Araki K, Erdogan F. Stress intensity factors in two bonded elastic layers with a single edge crack under various loading conditions. Int J Fract 1992; 57: 101-26.